Heterogeneity of the Human Pancreatic Islet

Michael P. Dybala and Manami Hara

Diabetes 2019;68:1230–1239 | https://doi.org/10.2337/db19-0072

Pancreatic β-cells play a pivotal role in maintaining normoglycemia. Recent studies have revealed that the β-cell is not a homogeneous cell population but, rather, is heterogeneous in a number of properties such as electrical activity, gene expression, and cell surface markers. Identification of specific β-cell subpopulations altered in diabetic conditions would open a new avenue to develop targeted therapeutic interventions. As intense studies of β-cell heterogeneity are anticipated in the next decade, it is important that heterogeneity of the islet be recognized. Many studies in the past were undertaken with a small sample of islets, which might overlook important individual variance. In this study, by systematic analyses of the human islet in two and three dimensions, we demonstrate islet heterogeneity in size, number, architecture, cellular composition, and capillary density. There is no stereotypic human islet, and thus, a sufficient number of islets should be examined to ensure study reproducibility.

Functional heterogeneity of β-cells in regard to glucose-responsive insulin secretion was reported decades ago (1–3). With the recent advancement of technologies, specialized pacemaker cells, termed "hubs," were identified as 1–10% of β-cells with a high degree of connectivity, high glucokinase, and low insulin, Pdx1, and Nkx6.1 expression (4). Similarly, molecular signatures of subpopulations of β-cells have been documented in maturation (Fltp [5], Srf [6], and Ucn3 [7]), proliferation (C1 [8]), and aging (IGF-IR [9]). Several other markers differentially expressed in subgroups of β-cells have also been reported, including PSA-NCAM (10), ST8SIA1 and CD9 (11), and MST1 (12). To date, all of these markers are solely claimed by each group of authors and not validated by other investigators. Therefore, relationships among these markers are still unknown (13). This is an exciting era in which new molecular insights of β-cell heterogeneity have begun to be revealed, which is thus currently one of the most focused areas in diabetes research.

Importantly, such heterogeneity extends to the pancreatic islet in its cytoarchitecture, particularly in humans, unlike in rodent islets (14–19). This heterogeneity of the human islet has not been systematically studied to date and thus may not have been properly recognized. It is well known that islets differ markedly in size throughout species from small to large islets consisting of thousands of endocrine cells. We have shown islet size–dependent variability in humans, including islet architecture, cellular composition, and intraislet capillary density (20). Humans can have 1 million islets (21). Many studies in the past were undertaken with only a few islets per donor. In some studies at single-cell levels, for example, ~50–70 cells were considered to represent one donor's endocrine pancreas, where a single islet with a 150-μm diameter can have ~1,000 cells.

The heterogeneity of the human pancreas is observed in four levels, in an ascending order: *1*) β-cell heterogeneity, *2*) islet heterogeneity, *3*) intraindividual regional variability of islet distribution, and *4*) interindividual heterogeneity. In this study, we aimed to show the islet heterogeneity in humans to demonstrate the need for baseline work, before exploring β-cell heterogeneity, by using a small number of so-called representative islets that have been somewhat allowed in the field. A study design inattentive to the aforementioned four levels of the heterogeneity of the human pancreas could result in misleading conclusions.

RESEARCH DESIGN AND METHODS

Human Pancreas Specimens

Human pancreata were provided by the Gift of Hope Organ & Tissue Donor Network Organ Procurement

Department of Medicine, The University of Chicago, Chicago, IL

Corresponding author: Manami Hara, mhara@uchicago.edu

Received 25 January 2019 and accepted 20 March 2019

This article contains Supplementary Data online at http://diabetes.diabetesjournals.org/lookup/suppl/doi:10.2337/db19-0072/-/DC1.

Organization in Chicago. Written informed consent from a donor or the next of kin was obtained for use of a sample in research. The use of deidentified human tissues in the study was approved by The University of Chicago Institutional Review Board. Over the course of developing a three-dimensional (3D) imaging method, several specimens were randomly used unless otherwise specified.

Mouse Pancreas Tissues

Pancreas tissues from 8-week-old C57BL/6J male mice were used. All of the procedures involving animals were approved by The University of Chicago Institutional Animal Care and Use Committee.

Antibodies

The following primary antibodies were used: mouse monoclonal anti-insulin (cat. no. ab8304, RRID:AB_2126399; Abcam, Cambridge, MA), mouse monoclonal anti-human glucagon (cat. no. WH0002641M1, RRID:AB_1841774; Sigma-Aldrich, St. Louis, MO), mouse monoclonal anti-somatostatin (cat. no. ab30788, RRID:AB_778010; Abcam), mouse monoclonal anti–pan-endocrine (HPi1; cat. no. MA5-16126, RRID:AB_11157008; Thermo Fisher Scientific, Waltham, MA), rabbit polyclonal anti-CD31 (cat. no. ab28364, RRID:AB_726362; Abcam), rabbit anti–α-smooth muscle actin (α-SMA; cat. no. ab5694, RRID:AB_2223021; Abcam), and DAPI (Invitrogen, Carlsbad, CA). The primary antibodies were conjugated with a combination of amine-reactive fluorophores (*N*-hydroxysuccinimide-esters; Thermo Fisher Scientific, Kalamazoo, MI).

Human Pancreas Imaging

A frozen human pancreas tissue block (~5 mm thick) was fixed in 4% paraformaldehyde, embedded in 2% agarose gel, and mounted on a vibrating microtome. Sections (600–800 μm thick) were collected in cold PBS. These macrosections were then immunohistochemically stained overnight. Optical clearing was performed by sequential incubation with 20, 50, 80, and 100% (w/v) solutions of D-fructose and 0.3% (v/v) α-thioglycerol (Sigma-Aldrich) for 1–2 h each at 35°C with gentle agitation. A Leica SP8 laser scanning confocal microscope was used to image tissue slices mounted between coverslips. 3D reconstruction and analysis were performed using Fiji and Imaris software (Bitplane, Concord, MA).

RESULTS

3D Visualization of Islet Heterogeneity

Human pancreatic islets were captured in situ in thick tissue slices (600–800 μm in depth). Shown in Fig. 1*A*a is a large-scale capture of a pancreatic tissue slice from a 13-year-old girl, immunostained for insulin (green), glucagon (cyan), CD31 (red), and α-SMA (yellow). Here, large blood vessels (i.e., arteries and veins) and arterioles are labeled with α-SMA (22). Note that most of the islets appear to have one feeding arteriole. This stack of multifluorescent images was surface rendered in 3D (Fig. 1*A*b), which provides solid views of the morphology of structures and the basis for volume quantification. Various sizes of islets were located along with arterioles (Fig. 1*B*). Also observed was heterogeneity in intraislet capillary density, which generally tended to be higher in larger islets (Fig. 1*C*), as we have previously reported (20).

3D Quantification of Endocrine Cell Composition in the Human Islet

The proportion of three major islet cells was quantified in 3D within intact pancreatic tissues. The total volume of individual islets was assessed by surface rendering of HPi1 staining [23]). A pancreatic tissue slice from a 24-year-old man was immunostained for insulin (green), glucagon (cyan), somatostatin (blue), and HPi1 (red) (Fig. 2*A*). Our 3D quantification method is shown step by step in Fig. 2*B–D* using a cluster of three islets boxed in Fig. 2*A*. First, fluorescent signals from the z-stack of all four channels were processed by binary conversion using Fiji (Fig. 2*B*). Next, the individual islet boundary was identified by 3D surface rendering of pan-endocrine fluorescent binary signal using Imaris (Fig. 2*C*a). Then, the volume of each islet and three types of endocrine cells was measured in 3D using fluorescent signals (Fig. 2*C*b–e). An example of z-stack views from top to bottom of islets is shown in Fig. 2*D*. Here, to recapitulate the common practice of selecting a small number of islets based on the idea of "the prototypical islet," five islets of different sizes were selected for each donor (Fig. 2*E*). The percentage of islet volume constituted by β-cells (insulin, green), α-cells (glucagon, cyan), and δ-cells (somatostatin, blue) was quantified. Marked intradonor islet variability was observed across a wide range of islets of varying volume.

Simulation of a Limited Selection of Islets From the Whole Human Pancreas

To recapitulate the common practice of selecting a small number of islets based on two-dimensional (2D) imaging and further demonstrate the resulting variance, we performed simulation by randomly selecting islets (as 1, 2, 3… up to 2,500 without replacement) from the whole human pancreas. Here we used previously characterized 10 age-matched male subjects without diabetes (21). The simulation workflow is shown in Fig. 3*A*. A subset of islets >40 μm in diameter was sampled from each of 10 subjects, and the average β-cell area was measured (Fig. 3*A*a). This sampling was repeated 1,000 times, and the mean β-cell area was plotted (Fig. 3*A*b). The total number of islets examined and subject information obtained from our previous study are provided. The distribution of β-cell composition by islet size was examined in three groups of islets according to a range of diameters (Fig. 3*A*c). Figure 3*B* depicts the simulation performed in the 10 human pancreatic samples. Mean ± SD and median β-cell area values are displayed for each donor. The distribution of β-cell composition sorted into three diameter ranges (100–

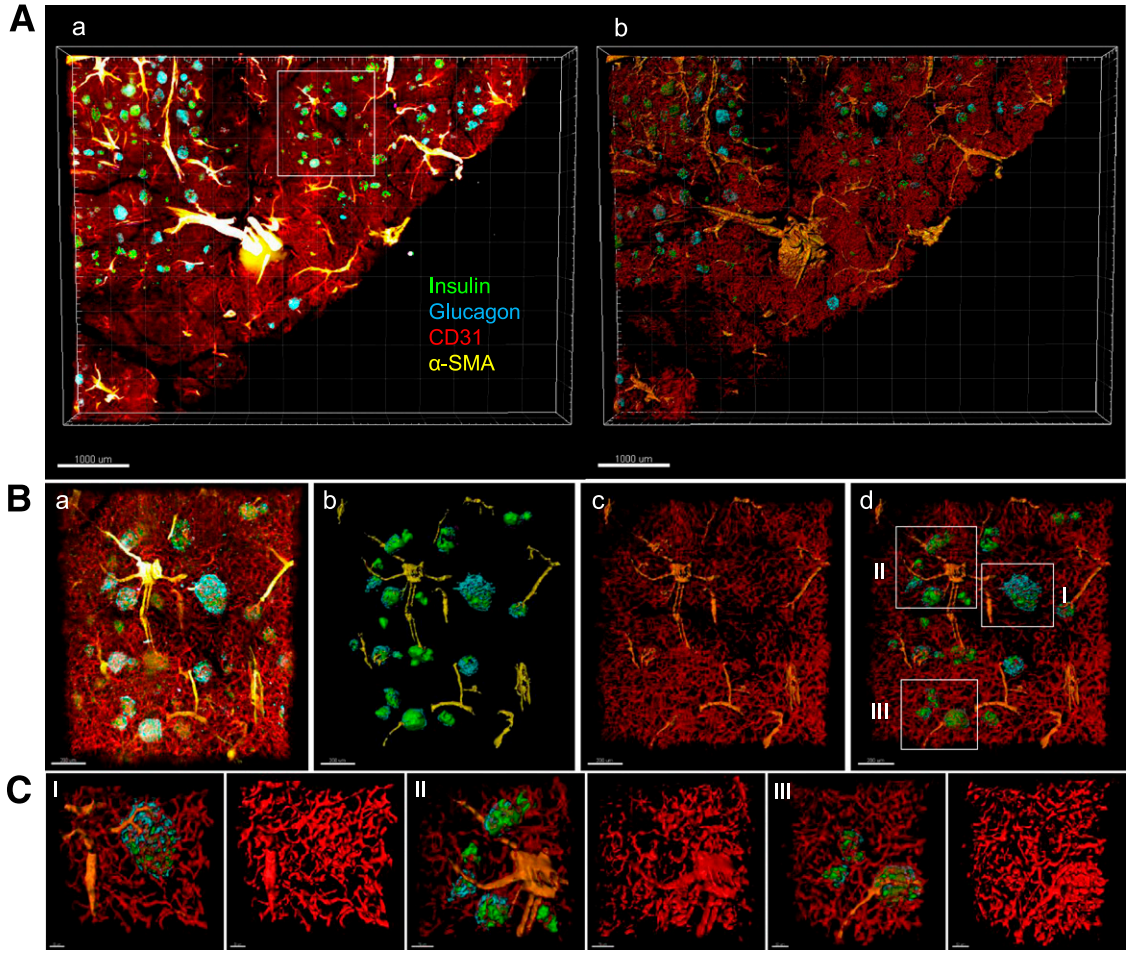

Figure 1—3D visualization of islet heterogeneity. *A*: (a) Large-scale image capture of a human pancreas tissue slice immunostained for insulin (green), glucagon (cyan), CD31 (red), and α-SMA (yellow). Scale bar: 1,000 μm. (b) 3D surface-rendered image of panel a. *B*: (a) Enlarged view of a cluster of various sizes of islets from the box in *A*a. (b) 3D surface-rendered image of panel a without blood vessels. (c) Blood vessels with α-SMA. (d) Large (I), intermediate (II), and small (III) islets selected for enlarged views. Note that blood vessels are made transparent to reveal underlying structures. Scale bars: all 200 μm. *C*: I, II, and III with images showing intraislet capillaries. Scale bars: all 20 μm.

200, 200–300, and 300–400 μm) revealed the extent of the islet heterogeneity within a similar size range in all individuals examined (Fig. 3*C*). Mean ± SD and median β-cell proportion for islets 100–200 μm in diameter are shown for each subject. A summary plot of the simulation in Fig. 3*D* provides the margin of error from the mean β-cell ratio of all islets in the pancreas depending on the number of islets sampled for each of 10 samples. Each point represents the difference between the mean β-cell ratio from a single sampling simulation for each sample size and the mean β-cell ratio of all islets from that subject. CIs for β-cell proportion are summarized in Table 1. Accordingly, to achieve a 95% CI of width of 5% around the mean β-cell ratio of the whole pancreas, a minimum of 400 islets would need to be examined to take the islet heterogeneity in humans into consideration. Importantly, note that the CIs are parameter specific. To assess the number of islets required for different parameters, large-scale data collection of individual measurements will be needed.

No Subunit Formation of the Mantle-Core Arrangement in the Human Islet

In 2D immunostaining, as shown in Fig. 4*A* (glucagon in red, insulin in green, and somatostatin in gray), mouse islets exhibit well-known mantle-core structure in that non–β-cells were mostly found in the periphery, although they do not form a complete mantle (Fig. 4*A*a). In human islets, non–β-cells are found in the core of islets, from small to large ones (Fig. 4*A*b–d), as has been previously documented (14–19). Note that α-cells were not randomly dispersed or scattered throughout the islets, as previously reported (14,15). Oftentimes, there appears to be a lining of α-cells surrounding a cluster of β-cells when observed in 2D slices, which has been referred to as "a subunit" resembling rodent islets (24–27). The authors noted that islets with higher proportions of β-cells (i.e., fewer α-cells) showed a clear pattern of such subunits of the rodent mantle-core organization, whereas some large islets with a lower proportion of β-cells (i.e., more α-cells) gave "the suggestion of random organization" with less clear subunit

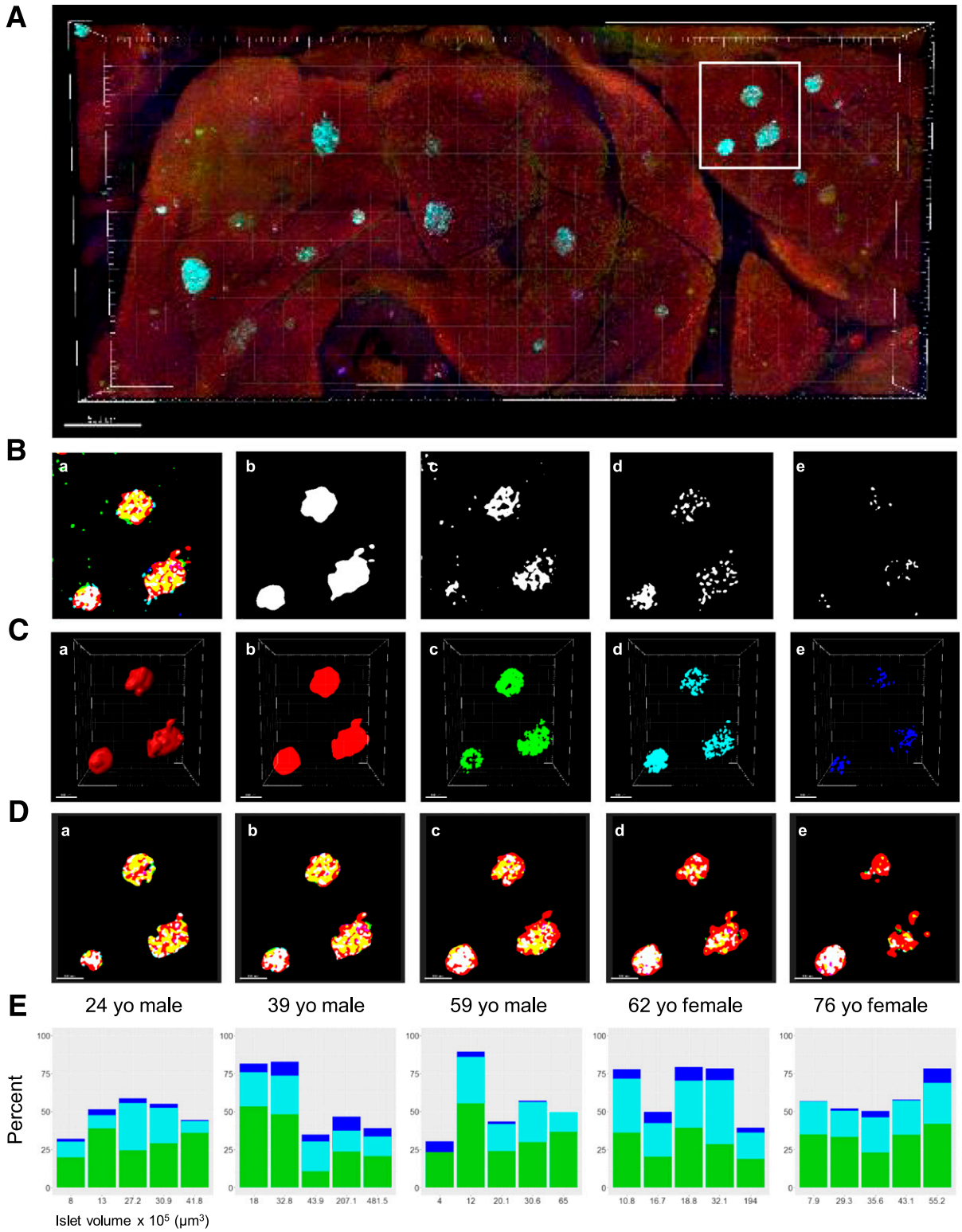

Figure 2—3D quantification of endocrine cell composition in the human islet. *A*: A large-scale capture of a tissue block immunostained for insulin (green), glucagon (cyan), somatostatin (blue), and a pan-endocrine cell surface marker (HPi1; red). Scale bar: 500 μm. *B*: Fluorescent signal processing of z-stack by binary conversion. (a) A representative slice of three islets (boxed in *A*) showing four channels merged. (b) Pan-endocrine. (c) Insulin. (d) Glucagon. (e) Somatostatin. *C*: Quantification of volume in 3D. (a) 3D surface rendering of pan-endocrine fluorescent binary signal used to identify islet boundary. 3D fluorescent signals for pan-endocrine (b), insulin (c), glucagon (d), and somatostatin (e). Scale bars: all 100 μm. *D*: (a–e) Optical slicing from top to bottom of islets showing pan-endocrine and three hormone fluorescent markers. *E*: Percentage of islet volume constituted by β-cells (insulin, green), α-cells (glucagon, cyan), and δ-cells (somatostatin, blue) was quantified. Five islets of different sizes were selected for each donor for quantification. yo, year-old.

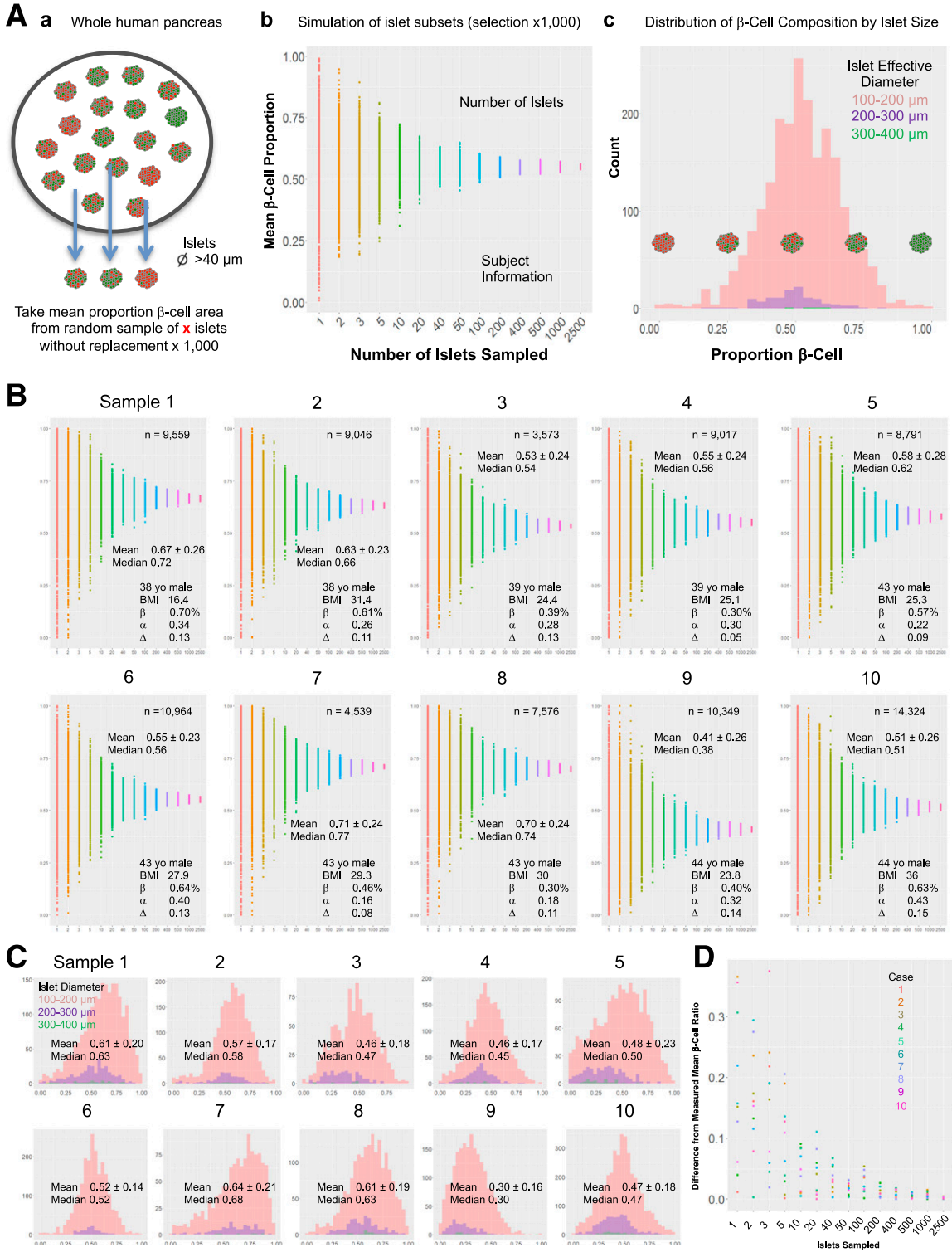

Figure 3—Simulation of the limited selection of islets out of the whole human pancreas. *A*: Workflow for sampling islets. (a) A subset of islets (>40 µm in diameter) was sampled from the whole human pancreas analysis (21), and the average β-cell area from 1,000 times sampling was measured. (b) Simulation of islet subsets showing the mean β-cell area. (c) Distribution of β-cell composition by islet size. *B*: Simulation performed in human pancreatic samples from 10 donors. Insets: the total number of islets examined and subject information. *C*: Distribution of β-cell composition sorted into three diameter ranges. *D*: Difference from mean β-cell proportion of all islets by simulated islet sample size from each of 10 donors. yo, year-old.

formation. Nonetheless, it was still considered that there was clear clustering of β-cells, "just smaller clusters" (27).

We hypothesized that depending on how a given islet was cut and imaged in 2D, some regions would show such structures. Therefore, we tried to reproduce similar 2D views by optically slicing a 3D z-stack image of solely the glucagon channel to highlight the lining of α-cells (Fig. 4*B*). Shown here are some optically sliced views from top to bottom (Fig. 4*B*a–f), 3D surface-rendered views of islets (Fig. 4*B*g), and the side views of g (Fig. 4*B*h). The first column depicts a mouse islet with a typical mantle-like pattern of α-cell distribution. However, no clear mantle-like pattern was observed in human islets. Here, we selected the above-mentioned two types of islets from three individuals. The amount of α-cells (i.e., larger or smaller proportion of an islet) was judged by 3D reconstructed views. The left column of each islet pair shows an islet with relatively fewer α-cells, and the right column shows an islet with more α-cells: I, a 16-year-old girl; II, a 59-year-old man; and III, a 62-year-old woman. In I, optical slicing of 3D z-stack images of a small islet with fewer α-cells may appear to be a rodent-like mantle pattern in selected 2D slices (Fig. 4*B*d–f). However, we failed to observe the same structure when this islet was reconstructed in 3D (Fig. 4*B*g and h). Interestingly, a larger islet with more α-cells showed subunit-like lining of α-cells (suggested by the aforementioned authors) in some of its 2D optical slices (Fig. 4*B*b–e). However, no rodent-like subunits were observed in 3D (Fig. 4*B*g and h). In the Supplementary Data, a montage of the entirety of optical slices of this islet (n = 90, 1 μm increment) is shown in Supplementary Fig. 1, together with a movie of the top-to-bottom view (Supplementary Movie 1). A 3D view of the islet is shown in Supplementary Movie 4. Similarly, as demonstrated in II and III, regardless of the proportion of α-cells, a certain lining of α-cells that may be suggestive of "a mantle-core pattern" can be observed depending on which optical plane was chosen in 3D as well as how a given islet was sectioned in 2D. We further captured a large islet (e.g., Feret diameter = 335 μm) with abundant α-cells in which a mantle-like structure was composed of a single layer of α-cells, which resembles the islet shown in Fig. 4*A*d. Note that the structure of α-cells found in these islets is rare. Montage and movies for II, III, and Fig. 4*C* are provided in the Supplementary Data (Supplementary Figs. 2–4 and Supplementary Movies 2, 3, and 5–11).

Islet Architecture and Capillary Bed

The 3D analysis also revealed an architectural relationship between different types of endocrine cells and the islet capillary bed. The limitation of 2D analysis is particularly evident for the network structure such as vasculature, neurons, and the extracellular matrix. Markers for all of these networks only appear as "dots" or "short lines" in 2D images of thinly cut sections, as we recapitulated such 2D views out of 3D imaging shown in Fig. 5*A*a–d. However, when these optical 2D slices were reconstructed in 3D,

Table 1—Width of 95% CI by number of islets sampled (β-cell ratio)

	Donor sample									
Islets sampled	1	2	3	4	5	6	7	8	9	10
2	0.51	0.547	0.421	0.589	0.809	0.923	0.252	1	0.545	0.52
3	0.34	0.511	0.489	0.909	0.906	0.887	0.548	0.905	0.692	0.999
5	0.69	0.371	0.566	0.52	0.813	0.658	0.384	0.818	0.783	0.863
10	0.394	0.361	0.423	0.305	0.277	0.35	0.211	0.308	0.426	0.215
20	0.244	0.262	0.145	0.199	0.207	0.105	0.179	0.23	0.181	0.25
40	0.173	0.172	0.132	0.153	0.141	0.139	0.168	0.138	0.139	0.136
50	0.15	0.184	0.116	0.114	0.129	0.134	0.141	0.143	0.155	0.134
100	0.103	0.108	0.097	0.086	0.102	0.088	0.096	0.1	0.096	0.114
200	0.076	0.079	0.067	0.054	0.06	0.065	0.065	0.06	0.074	0.069
400	0.051	0.054	0.048	0.046	0.047	0.047	0.047	0.047	0.05	0.053
500	0.046	0.048	0.043	0.042	0.042	0.041	0.041	0.043	0.043	0.046
1,000	0.032	0.035	0.029	0.03	0.029	0.03	0.03	0.031	0.033	0.032
2,500	0.02	0.022	0.018	0.018	0.019	0.019	0.019	0.019	0.02	0.021

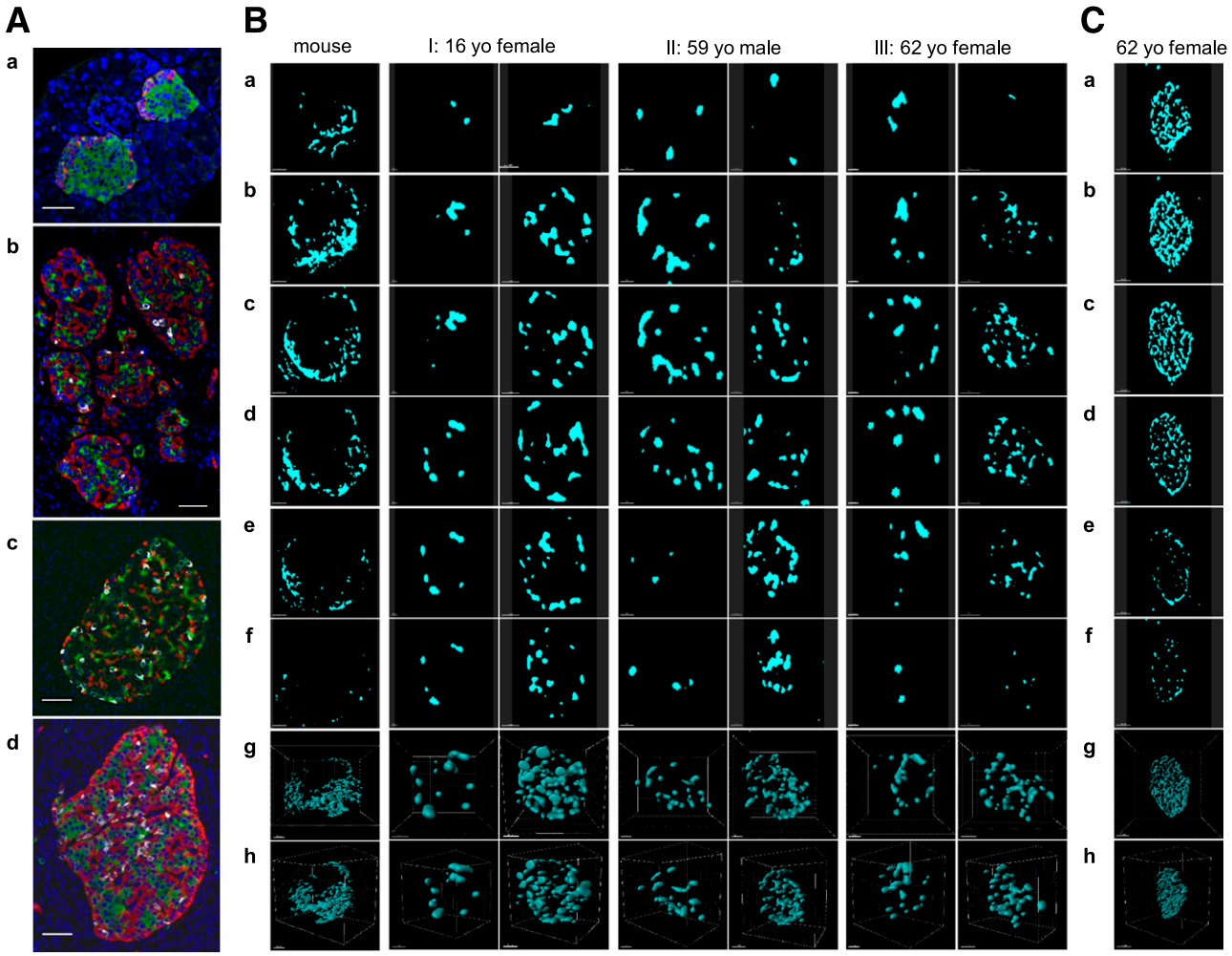

Figure 4—No subunit formation of the mantle-core arrangement in the human islet. *A*: 2D images of islets immunostained for insulin (green), glucagon (red), and somatostatin (white). (a) Mouse islets. Scale bar: 50 μm. (b) Human islets of various sizes. Scale bar: 50 μm. (c) Large islet. Scale bar: 50 μm. (d) Large islets. Scale bar: 100 μm. *B*: α-Cell distribution in mouse islets (8-week-old C57BL/6J) and human islets from three different donors (I: 16-year-old [yo] girl, II: 59-year-old man, III: 62-year-old woman). (a–f) Serial optical z-slices from top to bottom of the islet. Fluorescent signal for glucagon after binary conversion is shown. Front view (g) and side view (h) of 3D-rendered α-cells. Scale bar: 50 μm for mouse in a–f, 30 μm for mouse in g and h, all 30 μm for I except 20 μm for g, and all 20 μm for II and III. Scale bars: 30 μm for I except 50 μm for g and h, all 50 μm for II, and 20 μm for III except 40 μm for g and h. *C*: Serial z-slices of a large islet depicting glucagon signal from top to bottom and 3D rendering. (a–f) Top to bottom serial z-slices of islet showing binary converted fluorescence. (g) Front view of 3D-rendered α-cells. (h) Side view of g. Scale bar: 80 μm for a–f, 70 μm for g, and 100 μm for h. See also Supplementary Figs. 1–4 and Supplementary Movies 1–7.

vascular markers appearing once as dots or short lines resolved to a complex network of intraislet capillaries (Fig. 5*Ae* and f). Clustering of the same type of cells was observed, naturally to a higher extent for β-cells. Islet architecture varied throughout the size distribution, and all types of endocrine cells were capable of direct contact with islet capillaries (Fig. 5*B*–E). This is opposed to a previous report that α-cells were exclusively aligned along blood vessels (28).

DISCUSSION

The current study has demonstrated considerable islet heterogeneity and that there is no "stereotypic islet" in humans. Decades of research in rodent islets have concluded a somewhat stereotypical islet structure of a β-cell core with α- and δ-cells in the periphery. However, we have shown the atypical nature of the human islet, even within the same individual with regard to cellular composition as well as islet architecture. Endocrine cells are not dispersed or scattered throughout the human islets. Indeed, the predominant population of β-cells formed clusters within an islet, as did α-cells as well, to a lesser extent. We previously examined the relative attractions between islet endocrine cell types computationally and found that the attractions between homotypic cells were slightly, but significantly, stronger than the attractions between heterotypic cells, commonly in mouse, pig, and human islets (29). Interestingly, the difference between

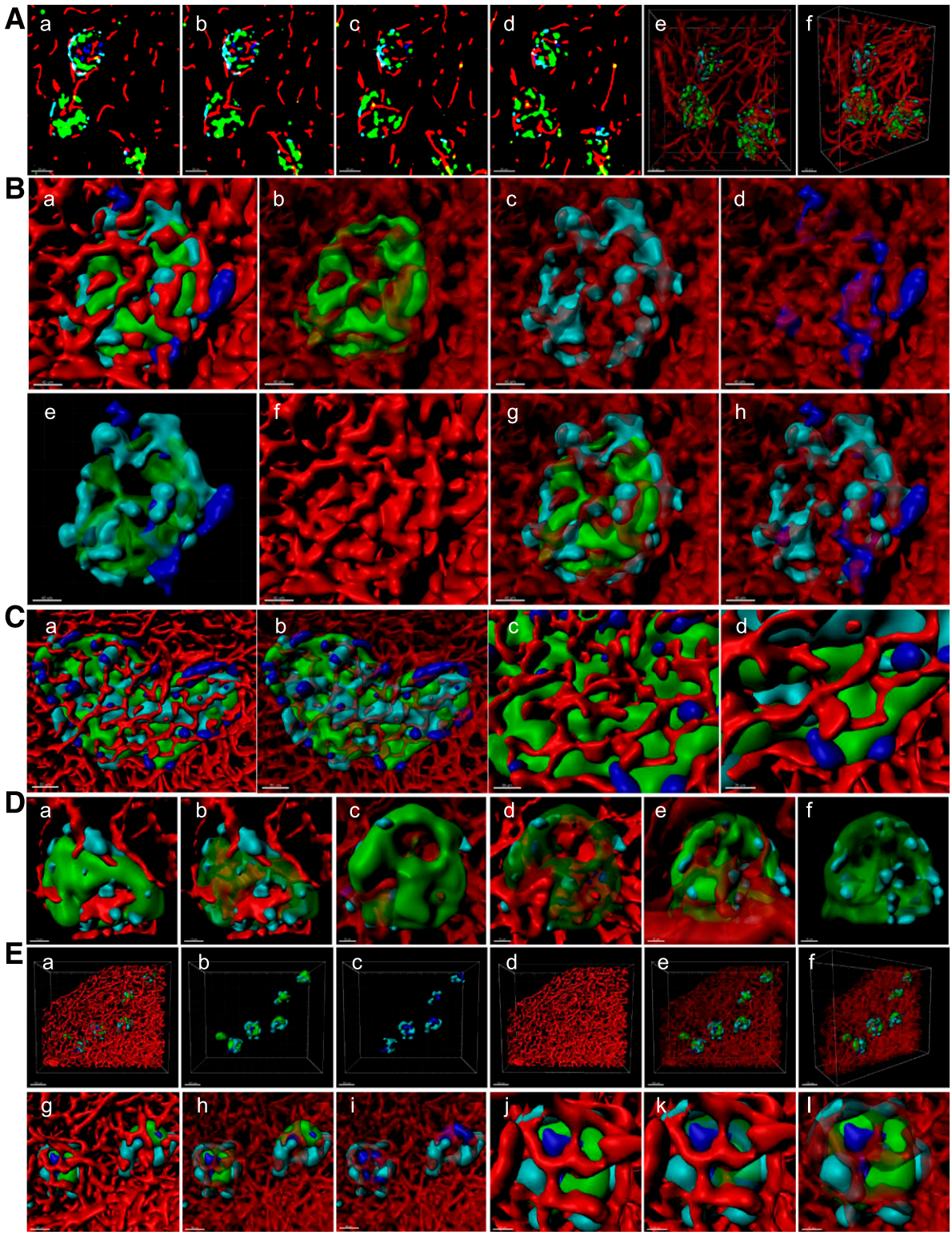

Figure 5—Islet architecture and capillary bed. *A*: (a–d) Sequential optical slices. Insulin (green), glucagon (cyan), somatostatin (blue), and CD31 (red). (e) 3D-reconstructed view of three islets and blood vessels. (f) Side view of e. Scale bars: all 50 μm. *B*: Intermediate size of islet (Feret diameter = 157 μm). (a) 3D-rendered view. Clusters of β-cells (b), α-cells (c), and δ-cells (d). (e) Endocrine cells only. (f) Blood vessels only. (g) β-Cells and α-cells. (h) α-Cells and δ-cells. Scale bars: all 40 μm. *C*: Large islet (Feret diameter = 404 μm). (a) 3D-rendered view. (b) Blood vessels made transparent. (c and d) Enlarged views. Scale bar: 50 μm for a and b, 30 μm for c, and 20 μm for d. *D*: Small islets. (a, c, and e) Solid 3D-rendered views. (b, d, and f) β-Cells made transparent. Scale bars: all 15 μm. *E*: A cluster of small islets. (a) 3D-rendered view. (b) β-Cells and α-cells. (c) α-Cells and δ-cells. (d) Blood vessels only. (e) 3D-reconstructed view with transparent blood vessels. (f) Side view of e. Scale bar: 100 μm for a–f, 40 μm for g–i, and 20 μm for j–l.

β-cell–to–α-cell attraction and β-cell–to–β-cell attraction was minimal in human islets, maximizing the plasticity of islet structures. Small islets usually have a low proportion of non–β-cells and thus tend to resemble the rodent mantle-core pattern; however, in this study, we also found some small islets with non–β-cells located in the center of islets. In addition, contrary to a report by Bosco et al. (28), vasculature penetrated small islets as well as the clusters of β-cells in larger islets. The authors also proposed "trilaminar epithelial plates" of islet organization, comprising one layer of β-cells sandwiched between two α-cell–enriched layers, and this structure should have a folded pattern and vessels circulate along both of its sides (28). We failed to observe such an organization in 3D.

An arrangement of rodent-islet-like subunit formation in the human islet has long been proposed, based on immunohistochemical analysis of thinly cut pancreatic tissue sections (24–27). Indeed, it had once been quite convincing, before the recent technological advancement of 3D analysis including microscopes, tissue clearing methods, and image analysis software. It may demonstrate our inability to reconstruct 2D phenomenon in 3D in the human brain in general. For example, we may tend to fill apparent gaps of the lining of α-cells as a continuous "mantle" and further extend it to an imaginative spherical structure in 3D (16). Such a phenomenon, in which the human brain perceives patterns as organized beyond their real presence, was recognized since as early as 1923, and described as the Gestalt Principles of Grouping (30). In the 3D analysis of the human pancreatic tissues, we did not find any rodent-islet-like subunit formation.

Unfortunately, heavy workload would not justify studies with an extremely small number of islets per donor. Such studies could lead to biased interpretations of experimental results and, therefore, would not ultimately benefit investigators themselves. Reasonable experimental design is the most important for the time and efforts undertaken for any studies. Then the question is how many islets out of a potential 1 million would represent the endocrine pancreas of one human. A range of "stereologically" appropriated numbers of islets to examine may depend on types of studies. In our study of β-cell/islet mass and islet number in the whole human pancreas, we first verified the frequency of sampling tissues (31). We found that with the unbiased examination of an entire tissue section, one section can sufficiently represent a pancreatic tissue block of ~1 cm in thickness from head to body to tail regions. Therefore, we divide a pancreas into consecutive blocks (~5 mm) with alternating collection between paraffin embedding and snap freezing. Then paraffin-embedded sections (5 μm) are used for computer-assisted quantification of β-cell/islet mass. While singly scattered endocrine cells and small clusters are always included, in this study, only islets >40 μm in diameter were examined for meaningful sizes of islets. The total number of islets examined in 10 cases was in a range of ~3,500–14,000 (average ± SD of 8,774 ± 3,078), reflecting the interindividual islet heterogeneity (32).

Our rationale for the whole pancreas analysis, despite its laborious effort, is based on the striking intraindividual regional variability of islet distribution (21,31,33,34). Studies including only a limited sample of pancreas may miss important variance both within the same pancreas and across individuals. Therefore, similarly, regarding islet heterogeneity, we propose that sufficient numbers of islets should be first explored in each experiment. Such pilot studies, while requiring certain significant commitment, should strengthen individual work in the long run. Studies using the state-of-art new technologies may be considerably expensive, labor intensive, and far from high throughput. On such occasions, rather than compromising with a small number of specimens, we should proactively seek for collaboration and further a nationwide and international consortium.

Computer modeling, including in silico screening, is suggested as one of the useful tools for the interrogation of β-cell heterogeneity by Benninger and Hodson (13). In their Perspective, the authors discussed the importance of using intact islets compared with dissociated endocrine cells, since interactions between cells within the islet are critical and tissue architecture influences gene expression. Furthermore, while enzymatic dissociation usually reduces cell viability with altered transcriptomic/protein features, the authors warn that some subpopulations with immature phenotypes, including hubs, appear more susceptible to endoplasmic reticulum stress and apoptosis/cell death. In fact, in the groundbreaking hubs study by Hodson and colleagues (4), a potential limitation of the study of recording Ca^{2+} oscillations in β-cells within a ~20-μm confocal plane, not in the entire islet, was compensated by mathematical modeling approaches such as Monte Carlo–based correlation analyses and power law link-probability distribution. The existing gaps in experiments between dissociated single cells and intact islets, as well as between isolated islets and islets in vivo, may be filled with computer modeling, at least to some extent.

In the very near future, with the anticipated rapid advancement of artificial intelligence (AI) and accompanied machine learning technology, many experimental approaches and techniques that have been believed to deserve "expertness and dedication of human beings" would be widely replaced with the AI, sooner or later. Importantly, biased data fed to the AI to teach a machine learning algorithm have been shown to significantly influence its behavior (the world's first psychopath AI [http://norman-ai.mit.edu/]). We propose that during this transitional era, it is critical to perform arduous but important baseline work in order to build the foundation for future studies.

Acknowledgments. The authors acknowledge Dr. Piotr Witkowski and Dr. J. Michael Millis at The University of Chicago, and Dr. Martin Jendrisak and the entire team of the Gift of Hope Organ & Tissue Donor Network in Chicago for providing the human pancreas tissues used in the current study.

Funding. The study was supported by National Institutes of Health, DK-117192 and DK-020595, to the University of Chicago Diabetes Research and Training Center (Physiology Core), DK-072473, and AG-042151, and a gift from the Kovler Family Foundation to M.H. Imaging was performed at The University of Chicago Integrated Light Microscopy Facility.

Duality of Interest. No potential conflicts of interest relevant to this article were reported.

Author Contributions. M.P.D. and M.H. performed tissue preparation, data collection and analyses, and manuscript preparation. M.H. designed the study. M.H. is the guarantor of this work and, as such, had full access to all the data in the study and takes responsibility for the integrity of the data and the accuracy of the data analysis.

Data and Resource Availability. All data generated or analyzed during this study are included in the published article (and its online Supplementary Data). No applicable resources were generated or analyzed during the current study.

References

1. Salomon D, Meda P. Heterogeneity and contact-dependent regulation of hormone secretion by individual B cells. Exp Cell Res 1986;162:507–520
2. Schuit FC, In't Veld PA, Pipeleers DG. Glucose stimulates proinsulin biosynthesis by a dose-dependent recruitment of pancreatic beta cells. Proc Natl Acad Sci U S A 1988;85:3865–3869
3. Kiekens R, In 't Veld P, Mahler T, Schuit F, Van De Winkel M, Pipeleers D. Differences in glucose recognition by individual rat pancreatic B cells are associated with intercellular differences in glucose-induced biosynthetic activity. J Clin Invest 1992;89:117–125
4. Johnston NR, Mitchell RK, Haythorne E, et al. Beta cell hubs dictate pancreatic islet responses to glucose. Cell Metab 2016;24:389–401
5. Bader E, Migliorini A, Gegg M, et al. Identification of proliferative and mature β-cells in the islets of Langerhans. Nature 2016;535:430–434
6. Qiu WL, Zhang YW, Feng Y, Li LC, Yang L, Xu CR. Deciphering pancreatic islet β cell and α cell maturation pathways and characteristic features at the single-cell level [published correction appears in Cell Metab 2018;27:702]. Cell Metab 2017;25:1194–1205.e4
7. van der Meulen T, Mawla AM, DiGruccio MR, et al. Virgin beta cells persist throughout life at a neogenic niche within pancreatic islets. Cell Metab 2017;25:911–926.e6
8. Wang YJ, Golson ML, Schug J, et al. Single-cell mass cytometry analysis of the human endocrine pancreas. Cell Metab 2016;24:616–626
9. Aguayo-Mazzucato C, van Haaren M, Mruk M, et al. β cell aging markers have heterogeneous distribution and are induced by insulin resistance. Cell Metab 2017;25:898–910.e5
10. Karaca M, Castel J, Tourrel-Cuzin C, et al. Exploring functional beta-cell heterogeneity in vivo using PSA-NCAM as a specific marker. PLoS One 2009;4:e5555
11. Dorrell C, Schug J, Canaday PS, et al. Human islets contain four distinct subtypes of β cells. Nat Commun 2016;7:11756
12. Ardestani A, Maedler K. MST1: a promising therapeutic target to restore functional beta cell mass in diabetes. Diabetologia 2016;59:1843–1849
13. Benninger RKP, Hodson DJ. New understanding of β-cell heterogeneity and in situ islet function. Diabetes 2018;67:537–547
14. Brissova M, Fowler MJ, Nicholson WE, et al. Assessment of human pancreatic islet architecture and composition by laser scanning confocal microscopy. J Histochem Cytochem 2005;53:1087–1097
15. Cabrera O, Berman DM, Kenyon NS, Ricordi C, Berggren PO, Caicedo A. The unique cytoarchitecture of human pancreatic islets has implications for islet cell function. Proc Natl Acad Sci U S A 2006;103:2334–2339
16. Kharouta M, Miller K, Kim A, et al. No mantle formation in rodent islets – the prototype of islet revisited. Diabetes Res Clin Pract 2009;85:252–257
17. Kim A, Miller K, Jo J, Kilimnik G, Wojcik P, Hara M. Islet architecture: a comparative study. Islets 2009;1:129–136
18. Steiner DJ, Kim A, Miller K, Hara M. Pancreatic islet plasticity: interspecies comparison of islet architecture and composition. Islets 2010;2:135–145
19. Kilimnik G, Jo J, Periwal V, Zielinski MC, Hara M. Quantification of islet size and architecture. Islets 2012;4:167–172
20. Fowler JL, Lee SS, Wesner ZC, Olehnik SK, Kron SJ, Hara M. Three-dimensional analysis of the human pancreas. Endocrinology 2018;159:1393–1400
21. Olehnik SK, Fowler JL, Avramovich G, Hara M. Quantitative analysis of intra- and inter-individual variability of human beta-cell mass. Sci Rep 2017;7:16398
22. Silverthorn DU. Blood flow and the control of blood pressure. In *Human Physiology: An Integrated Approach*. 8th ed. Cechvala C, Harp L, Eds. Hoboken, NJ, Pearson, 2018, p. 562–598
23. Dorrell C, Abraham SL, Lanxon-Cookson KM, Canaday PS, Streeter PR, Grompe M. Isolation of major pancreatic cell types and long-term culture-initiating cells using novel human surface markers. Stem Cell Res (Amst) 2008;1:183–194
24. Orci L, Unger RH. Functional subdivision of islets of Langerhans and possible role of D cells. Lancet 1975;2:1243–1244
25. Erlandsen SL, Hegre OD, Parsons JA, McEvoy RC, Elde RP. Pancreatic islet cell hormones distribution of cell types in the islet and evidence for the presence of somatostatin and gastrin within the D cell. J Histochem Cytochem 1976;24:883–897
26. Grube D, Eckert I, Speck PT, Wagner HJ. Immunohistochemistry and microanatomy of the islets of Langerhans. Biomed Res 1983;4(Suppl.):25–36
27. Bonner-Weir S, Sullivan BA, Weir GC. Human islet morphology revisited: human and rodent islets are not so different after all. J Histochem Cytochem 2015;63:604–612
28. Bosco D, Armanet M, Morel P, et al. Unique arrangement of alpha- and beta-cells in human islets of Langerhans. Diabetes 2010;59:1202–1210
29. Hoang DT, Matsunari H, Nagaya M, et al. A conserved rule for pancreatic islet organization. PLoS One 2014;9:e110384
30. Wertheimer M. Untersuchungen zur Lehre von der Gestalt. II. Psychologische Forschung 1923;4:301–350
31. Poudel A, Fowler JL, Zielinski MC, Kilimnik G, Hara M. Stereological analyses of the whole human pancreas. Sci Rep 2016;6:34049
32. Dybala MP, Olehnik SK, Fowler JL, et al. Pancreatic beta cell/islet mass and body mass index. Islets 2019;11:1–9
33. Poudel A, Savari O, Striegel DA, et al. Beta-cell destruction and preservation in childhood and adult onset type 1 diabetes. Endocrine 2015;49:693–702
34. Wang X, Zielinski MC, Misawa R, et al. Quantitative analysis of pancreatic polypeptide cell distribution in the human pancreas. PLoS One 2013;8:e55501